Exchange bias in self-organized nanopatterned Cr/Fe junctions

F. Bisio,* L. Anghinolfi, M. Canepa, and L. Mattera
Dipartimento di Fisica and CNISM, Sede Consorziata di Genova, Università di Genova, via Dodecaneso 33, I-16146 Genova, Italy
(Received 19 December 2008; revised manuscript received 8 January 2009; published 6 February 2009)

We have investigated the exchange bias (EB) in ultrathin epitaxial Cr/Fe/Ag(001) nanopatterned bilayers characterized by atomic-scale-tailored interfaces consisting of nanoripples aligned along the $[100]_{Fe}$ direction. Precisely measuring the magnetic anisotropy of the system, we quantitatively characterized the energetics of the magnetization reversal in terms of domain-wall propagation in the Fe layer and discussed the influence of the interface structure in determining the exchange bias and promoting the domain-wall processes. We found no influence of the relative orientation of the field-cooling direction with respect to the nanoripple orientation in determining the EB magnitude, but we observed that the anisotropic morphology generates characteristic spin frustrations affecting the energetics of different domain-wall processes.

DOI: 10.1103/PhysRevB.79.054407 PACS number(s): 75.30.Et, 75.75.+a, 75.60.Jk

I. INTRODUCTION

Composite materials consisting of contacted ferromagnetic (FM) and antiferromagnetic (AF) substances exhibit a variety of extremely interesting properties due to the exchange interaction between the two materials.[1–3] Among them, exchange bias (EB), a characteristic unidirectional anisotropy observed after field cooling (FC) the system through the Néel temperature of the AF, has been for decades attracting a tremendous amount of experimental and theoretical attention.[1,2,4–7]

Despite the efforts made, a comprehensive understanding of EB has yet to emerge. The reasons for such a lack of a general picture are multiple. The short-ranged nature of the exchange interaction makes EB extremely sensitive to the occurrence of even atomic-scale imperfections at the FM-AF interface, the characterization of the magnetic state of the AF is extremely difficult to perform, and the overall magnetic anisotropy energy (MAE) and domain state of the system have to be well known in order to model its properties. Early experimental works on EB have been performed on systems whose MAE or interface morphology were not sharply defined, thereby leaving many of the above issues with no definite answer, whereas experiments performed on AF-FM systems with tailored MAE and/or interfacial morphology/structure are recently starting to positively contribute to clarifying these points.[7–12]

In this paper we address the EB properties of ultrathin epitaxial nanopatterned Cr/Fe/Ag(001) multilayers characterized by atomic-scale-engineered interface morphology. The surface of the Fe layer was nanopatterned by the ion sculpting technique[13] prior to the Cr growth to create nanometric-sized *crystalline* ripples coherently aligned along the $[100]_{Fe}$ direction (see Fig. 1), thus providing a well-defined interface between the materials consisting of $[100]_{Fe}$-aligned monatomic steps. Precisely measuring the MAE of the FM layer, we reliably modeled the magnetization properties of the system and selectively pinpointed the influence of the interface structure on exchange bias. We found a negligible role of interface steps in determining the EB magnitude, whereas the anisotropic morphology generates characteristic spin frustrations affecting the energetics of different domain-wall (DW) processes.

II. EXPERIMENTAL

The experiments have been performed in an ultrahigh vacuum (UHV) chamber ($p<1\times10^{-10}$ mbars) featuring *in situ* MOKE, as well as facilities for ultra-thin-film growth and characterization.[14] The *in situ* magnetic field **H** for MOKE measurements is provided by means of an electromagnet whose poles reach inside the UHV chamber. Careful calibration of the electromagnet and highly controlled MOKE experimental procedures allow one to reliably measure hysteresis loops with ±0.4 Oe resolution in **H**. A sample morphology schematically sketched in the top part of Fig. 1 is obtained as follows. Epitaxial Fe films of thickness $t_{FM}=30$ Å were deposited by molecular-beam epitaxy onto a clean and flat Ag(001) according to established procedures.[15,16] Fe grows on Ag with epitaxial relations $[100]_{Fe}\|[110]_{Ag}$ and $[001]_{Fe}\|[001]_{Ag}$.[17] Once deposited, the self-organized formation of surface ripples onto the Fe surface was induced by means of the well-established ion

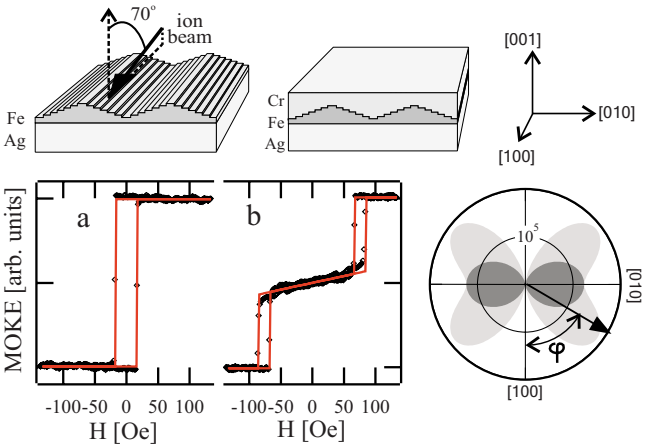

FIG. 1. (Color online) Top: sketch of the ripple morphology of nanopatterned Cr/Fe/Ag(001) bilayers. Bottom left: magneto-optical Kerr effect (MOKE) hysteresis loops measured for as-deposited Cr/Fe/Ag(001) bilayers (external field (a) $\mathbf{H}_{ext}\|[100]_{Fe}$ and (b) $\mathbf{H}_{ext}\|[010]_{Fe}$). Bottom right: angular dependence of the MAE deduced from loop b (light gray); in dark gray the uniaxial anisotropy K_u.

sculpting technique,[13] irradiating the film at $T=350$ K by means of a defocused beam of 1 KeV Ar^+ ions incident at 70° from the surface normal and along the $[100]_{Fe}$ direction,[16] as schematically shown in Fig. 1. After 5×10^{12} ions/cm^2 fluence, the Fe surface morphology, as determined in Ref. 16 by means of spot-profile-analysis low-energy electron diffraction (LEED), consisted of ripples with ridges oriented along $[100]_{Fe}$ with mean wavelength $\Lambda\approx9$ nm, whose side walls consisted of crystalline facets at a mean angle $\alpha\approx14°$ with respect to the surface normal. Under these conditions, the Fe ripples are not separated but rather represent a regular and coherently oriented undulation of an otherwise continuous Fe film.[16] From the mean value of ripple wavelength and side-wall slope reported above, an average of approximately ten exposed Fe layers within each ripple can be expected.

Epitaxial 45-Å-thick Cr films were deposited, by molecular-beam epitaxy, on the rippled Fe surface at $T=160$ K. The low-temperature growth is expected to strongly inhibit the intermixing between the Cr overlayer and the underlying Fe film, resulting in a sharp interface between the materials. The absence of significant blurring of the buried Cr/Fe interface was confirmed by the analysis of the stability of the magnetic anisotropy properties of the bilayers, as discussed in deeper detail in Ref. 18. Cr films grow epitaxially on Fe (Cr/Fe epitaxial relations $[100]_{Fe}\|[100]_{Cr}$ and $[001]_{Fe}\|[001]_{Cr}$ (Ref. 19)). The very small lattice mismatch between Cr and Fe, together with the fact that both elements have the same crystallographic structure (body-centered cubic), favors the good epitaxial growth of Cr on Fe even in the presence of surface ripples on the Fe films, as confirmed by the observation of LEED patterns with well-defined diffraction spots from the bilayer structure at all stages of growth. After deposition, the Cr surface was exposed to 20 L (1 L $=1\times10^{-6}$ mbar s) of research-grade O_2 and annealed at 670 K. This procedure induced the formation of an extremely thin chromium oxide layer, as checked by Auger spectroscopy, that did not affect the underlying Fe layer but effectively prevented any further sample contamination, thereby making the sample properties extremely stable for long periods of time.[18] We remark that the stepped Cr/Fe interface fabricated via the above-specified procedures, together with the well-known layered-AF character of Cr {001} planes, is expected to yield a compensated interface. All the data reported have been measured with the sample held under UHV conditions.

Longitudinal MOKE hysteresis loops measured with *s*-polarized light at $T=150$ K for the Cr/Fe/Ag bilayer in the as-grown state are reported in Fig. 1, bottom graph, for applied field $\mathbf{H}_{ext}\|[100]_{Fe}$ and $\mathbf{H}_{ext}\|[010]_{Fe}$ (left and right, respectively). These loops, being symmetric with respect to $\mathbf{H}_{ext}=0$ in the as-grown state, exhibit no exchange bias. However, their analysis provides important information about the MAE of the system, its FM domain structure, and the magnetization reversal process. In particular we notice that whereas loop "a" is square, loop "b" exhibits a very characteristic split shape, with zero remanence and two semiloops symmetrically shifted by approximately 75 Oe with respect to the $\mathbf{H}=0$ axis. Such a peculiar shape, as shown in a number of studies,[16,20–22] is indicative of a total system's MAE given by the superposition of a biaxial anisotropy contribution (K_c), having an easy axis of magnetization pointing along the $[100]_{Fe}$ and crystallographic equivalent directions, and a uniaxial (K_u) contribution favoring the magnetization alignment parallel to $[100]_{Fe}$. In our case, the K_c and K_u contributions, respectively, arise from the *effective* in-plane biaxial anisotropies of the combined Fe and Cr films, and from the step-induced interface anisotropy due to the nanoripples.[16,18,23] Both loops exhibit very sharp irreversible transitions, thereby suggesting that the magnetization reversal process proceeds by transitions between single-domain Fe states mediated by DW nucleation and subsequent propagation.[24] For systems with the above-described MAE, when the externally applied field is $\mathbf{H}_{ext}\|[100]_{Fe}$ ($\mathbf{H}_{ext}\|[010]_{Fe}$) directions, the magnetization reversal takes place via propagation of 180° (90°) DWs.[20] For $\mathbf{H}_{ext}=140$ Oe the Fe magnetization is clearly saturated for both $\mathbf{H}_{ext}\|[100]_{Fe}$ and $\mathbf{H}_{ext}\|[010]_{Fe}$. We point out that, given the *continuous* nature of the rippled Fe film, the magnetic domains within the films span over an extremely large number of nanoripples and that, accordingly, the magnetization reversal process does not by any means proceed by individual nanoripple reversal. Furthermore, we stress that the characteristic shape of the loops reported in Fig. 1 simply arises from a magnetic anisotropy effect and that no exchange bias was detected in the as-deposited state.

In order to extract quantitative information about the MAE of our system from the hysteresis loops, we write the anisotropic part of the free-energy density of the unbiased system as

$$f=\frac{K_c}{4}\sin^2(2\varphi)+K_u\sin^2(\varphi)-\mathbf{M}\cdot\mathbf{H}_{ext}, \tag{1}$$

where φ is the angle between the magnetization $\mathbf{M}$ and the $[100]_{Fe}$ direction and $\mathbf{M}=1752$ emu/cm^3. The hysteresis loops are modeled by locally minimizing f with respect to φ for any given $\mathbf{H}_{ext}$; DW processes are included in the model by holding $\mathbf{M}$ in a pertinent local minimum $\bar{\varphi}$ of f until a global minimum of f is found at $\hat{\varphi}$ satisfying the condition $[f(\bar{\varphi})-f(\hat{\varphi})]\geq E_{DW}^{90(180)}$, with $E_{DW}^{90(180)}$ being the activation energy for the appropriate DW process. Fitting the model loop to the experimental data allows one to determine, from the $\mathbf{H}_{ext}\|[010]_{Fe}$ case, K_c, K_u, and E_{DW}^{90}, while E_{DW}^{180} is deduced from the $\mathbf{H}_{ext}\|[100]_{Fe}$ case. We remark that the E_{DW} that we extract from this simple model corresponds to the onset of the *sharp* switching of the magnetization direction.

The hysteresis loops corresponding to the best-fit procedure (red lines in the graph of Fig. 1) yielded $K_c=(3.3\pm0.3)\times10^5$ erg/cm^3, $K_u=(1.35\pm0.05)\times10^5$ erg/cm^3, $E_{DW}^{90}/\mathbf{M}=8.5$ Oe, and $E_{DW}^{180}/\mathbf{M}=16.9$ Oe. The corresponding functional form of the system MAE is reported in the bottom-right part of Fig. 1. The good agreement with experiment confirms the correctness of our assumptions, whereas we point out that a simpler coherent-rotation model leads to unrealistic values for the anisotropy.

Having determined the MAE of our sample and characterized the magnetization reversal process, we move forward to determine whether the strongly anisotropic structure and

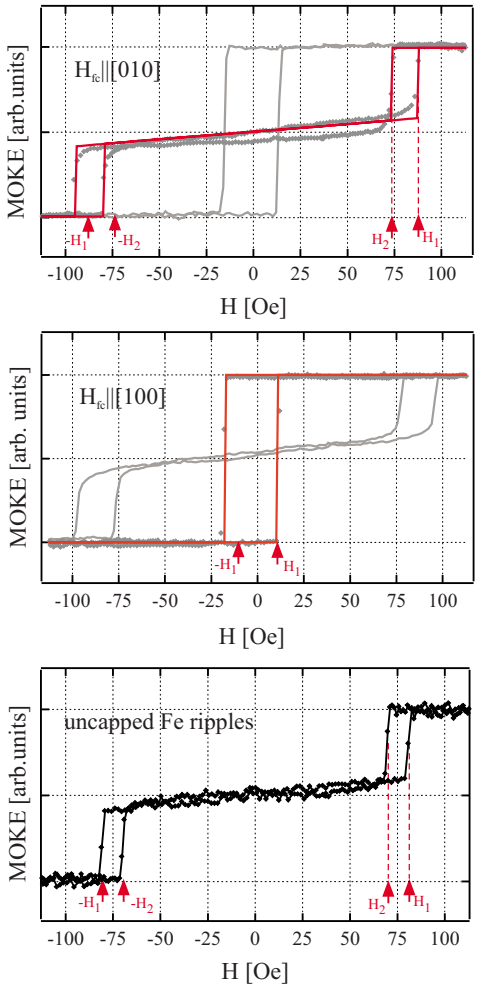

FIG. 2. (Color online) Top: hysteresis loops measured for $\mathbf{H}_{FC}\|[010]_{Fe}$ for the Cr/Fe/Ag(001) bilayer. External field $\mathbf{H}_{ext}\|[010]_{Fe}$ (symbols) and $\mathbf{H}_{ext}\|[100]_{Fe}$ (gray line). Red line: best-fit simulated loop. Middle: hysteresis loops measured for $\mathbf{H}_{FC}\|[100]_{Fe}$ for the Cr/Fe/Ag(001) bilayer; external field $\mathbf{H}_{ext}\|[100]_{Fe}$ (symbols) and $\mathbf{H}_{ext}\|[010]_{Fe}$ (gray line). Red line: best-fit simulated loop. Bottom: hysteresis loops measured for $\mathbf{H}_{FC}\|[010]_{Fe}$ for the Fe/Ag(001) nanopatterned film prior to the deposition of Cr. The red arrows in the graphs are drawn in symmetrical position with respect to the $\mathbf{H}_{ext}=0$ axis in all panels in order to help appreciate the loop shift.

morphology of our sample has a corresponding effect on its EB characteristics. Field-cooling procedures were then performed on the nanopatterned multilayer for in-plane field $\mathbf{H}_{FC}$ either parallel or perpendicular to the ripple orientation. The external field was set in both cases at $\mathbf{H}_{FC}=+140$ Oe, and the FC was performed from $T=670$ to 168 K.

In the top panel of Fig. 2 we report two MOKE hysteresis loops measured at $T=165$ K with $\mathbf{H}_{ext}\|[010]_{Fe}$ (symbols) and $\mathbf{H}_{ext}\|[100]_{Fe}$ (gray line) after a FC with $\mathbf{H}_{FC}\|[010]_{Fe}$. The loop measured with $\mathbf{H}_{ext}\|[010]_{Fe}$ has retained its split shape, with slightly rounded onsets of the irreversible transitions, and exhibits a small yet clear shift $\mathbf{H}_{EB}\approx(3.6\pm0.4)$ Oe toward the negative direction of the magnetic field axis. Ascending and descending branches of the loop have identical shape; the asymmetric slope in the low-field region is due to second-order magneto-optical effects[25] and not to EB. Other loops, measured for several orientations of $\mathbf{H}_{ext}$ with respect to the ripple directions (not shown), also exhibit various degrees of asymmetry, as expected for anisotropic EB systems,[9,10] while the loop measured for $\mathbf{H}_{ext}\|[100]_{Fe}$ is symmetric.

We modeled the biased hysteresis loops simply by adding to Eq. (1) a unidirectional contribution $f_{EB}=(J/t_{FM})\cos(\varphi+\varphi_{EB})$ and optimizing its magnitude and in-plane orientation by comparison with experiment; the best agreement between data and simulations (red line in Fig. 2) was found for $J=(1.7\pm0.2)\times10^{-3}$ erg/cm^2 and $\varphi_{EB}=\pi$ (i.e., easy unidirectional axis pointing toward $[010]_{Fe}$). The good agreement with experiment suggests that our model still holds for the biased system, meaning we can *directly* access the activation energy of specific DW processes in the presence of EB, an extremely important outcome given the importance of DW processes in EB systems.[26–29]

The hysteresis loops measured at $T=165$ K after performing a FC with $\mathbf{H}_{FC}\|[100]_{Fe}$ are instead reported in the middle panel of Fig. 2 for $\mathbf{H}_{ext}\|[100]_{Fe}$ (symbols) and $\mathbf{H}_{ext}\|[010]_{Fe}$ (gray line). The loop recorded with $\mathbf{H}_{ext}\|\mathbf{H}_{FC}$ has preserved its square shape, with sharp irreversible transitions, and has shifted toward the negative end of the field axis by $\mathbf{H}_{EB}\approx(3.5\pm0.2)$ Oe. Various asymmetries are also observed when changing the relative angle between $\mathbf{H}_{ext}$ and $\mathbf{H}_{FC}$, not completely disappearing even in the *longitudinal* loop measured for $\mathbf{H}_{ext}\|[010]_{Fe}$. Introducing again f_{EB} in Eq. (1), we find good agreement with experiment for (red line on bottom graph) $J=(1.7\pm0.1)\times10^{-3}$ erg/cm^2 and $\varphi_{EB}=-\pi/2$ (i.e., easy unidirectional axis pointing toward $[100]_{Fe}$).

Though small, the shift of the exchange-biased hysteresis loops is well reproducible fully within the sensitivity of our setup and free of systematic experimental artifacts. This fact can be even better appreciated comparing, e.g., the exchange-biased loops reported in the top panel of Fig. 2 with a reference loop measured, with $\mathbf{H}_{ext}\|[010]_{Fe}$, just prior to the deposition of the Cr overlayer on the Fe nanorippled film ($T=160$ K) reported in the bottom panel of Fig. 2. There, the symmetry of the irreversible magnetization jumps with respect to the $\mathbf{H}_{ext}=0$ axis is apparent, thereby confirming the observation of EB in the field-cooled loops.

The temperature dependence of J for $\mathbf{H}_{FC}\|[010]_{Fe}$ and $\mathbf{H}_{FC}\|[100]_{Fe}$ is reported in Fig. 3, top panel; J vanishes in both cases for a blocking temperature T_b in the close vicinity of 300 K, with T_b being seemingly higher, by roughly 10 K, for the $\mathbf{H}_{FC}\|[010]_{Fe}$ case. The temperature dependences of the DW activation energies of $2\times E_{DW}^{90}$ (corresponding to a full magnetization reversal) and E_{DW}^{180}, respectively, measured for $\mathbf{H}_{FC}\|[010]_{Fe}$ and $\mathbf{H}_{FC}\|[100]_{Fe}$, are instead reported in the bottom panel of Fig. 3. The data reveal a strong similarity of J for the two-orthogonal FC direction, whereas more different temperature dependences between E_{DW}^{90} and E_{DW}^{180} appear all over the investigated temperature range, more evident in proximity of T_b.

III. DISCUSSION

The values of the interfacial coupling J reported for Cr/Fe in the literature span a relatively large interval;[30–32] our value

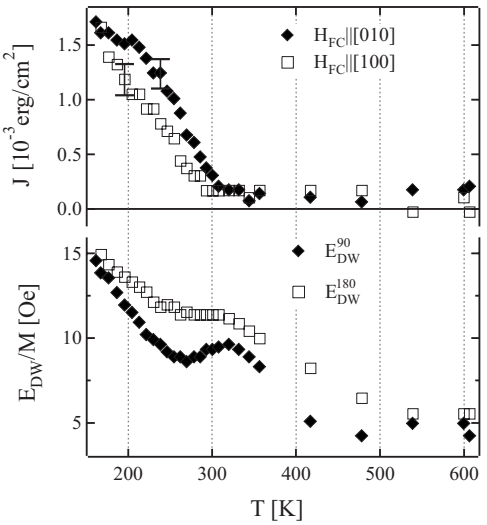

FIG. 3. Temperature dependence of the interface coupling J (top) and E_{DW} (bottom) for $\mathbf{H}_{FC}\|[010]$ (full diamonds) and $\mathbf{H}_{FC}\|[100]$ (open squares).

agrees fairly well with most of such values,[30,31] resulting, however, smaller than others.[32] The strong interface-morphology dependence of J does not allow an easy comparison with samples fabricated under different conditions, and we will accordingly not discuss in depth the value of J in itself. We will instead focus our attention on the very weak dependence of J on the FC direction in our sample, which is a relatively unexpected finding, given the extremely strong atomic-scale structural anisotropy of the Cr/Fe interface and the well-known occurrence of complex spin frustrations in this system taking place in correspondence of interface atomic steps.[33–35]

It is well known that the EB effect arises because of a limited fraction of interfacial uncompensated spins, whose direction stays pinned while the FM magnetization rotates.[32,36,37] In this framework, our data clearly indicate that, irrespective of the relative orientation between $\mathbf{H}_{FC}$ and the nanoripples, the density of uncompensated spins effective for determining the EB stays the same. We accordingly interpret this observation supposing that the spins located in contact with $[100]_{Fe}$-aligned straight steps give rise to null EB for both FC orientations. Whereas this finding can be naively understood stressing the intrinsically compensated nature of neighboring {001} Cr planes, it provides the important indication that no matter how complex the frustrated-spin configuration in proximity of atomic steps and its dependence on the underlying FM magnetization orientation is, it yields no uncompensated spins. If straight atomic steps are not contributing the uncompensated pinned-spin fraction, such spins could be likely found in proximity of structural/morphological imperfections of the sample, as occurring for several other EB systems.[7,36] Such areas of the sample cannot be grain boundaries or similar defects in substrate or films, given their single crystal and epitaxial character, respectively, but can be likely identified as morphological defects of the ripple structure,[13] where a local breakdown of the strong morphological and structural uniaxial symmetries of the sample takes place. In this simple picture, the magnitude of the EB for the two in-plane-orthogonal FC directions would substantially be independent of the orientation of the interface steps, as experimentally observed.

Concerning the domain-wall activation energies E_{DW}, a very interesting feature is represented by the observation of different activation energies for 90°- and 180°-DW processes, and of a correspondingly different temperature dependence. We begin the discussion by pointing out that for the system under analysis here, the DW activation energy, and hence the observed coercivity, does not bear a straightforward relation with the sample MAEs, as would occur in systems whose behavior can be modeled with coherent magnetization reversal processes.[38] The onset of the magnetization reversal in our sample, starting with the nucleation of a reversed domain in the film, is instead much more dependent on both the morphological and the spin state of the sample since morphologically or magnetically "defective" sites typically act as favorite nucleation centers for DWs that successively propagate through the film.[24,26,39] For 180°-DW processes, we systematically observe very sharp onset of the magnetization "jump," indicating that DW propagation sets in as soon as a reverse domain nucleates.[24] In contrast, 90°-DW processes apparently proceed by diffuse nucleation of reverse domains (the rounded onsets of irreversible transitions) that eventually propagate through the film when a critical field is reached. Since the morphological quality of the sample is identical for 90° or 180° DWs and the sample MAE is appropriately accounted for, the different behavior of the two types of DWs has to be ascribed to a spin-dependent effect. Let us therefore suppose that the preferential sites for reversed-domain nucleation are the sites at which, according to the above hypothesis, the uncompensated biased spins are concentrated. The characteristic energies for nucleating (propagating) 90°-reversed domains or 180°-reversed domains in the FM layer are influenced by the exchange-coupling strength between such uncompensated spins and the spins of the FM layers. The strong dependence of the exchange energy on the angle between $\mathbf{M}$ and the AF uncompensated spins would then naturally give rise to a different nucleation/propagation energy for 90°- or 180°-reversed domains. In this respect, E^{90}_{DW} is systematically lower than E^{180}_{DW}, indicating less stable configurations for the former case; we propose that this is due to the fact that when 90°-DW processes are involved, the system probes, at different stages of the magnetization reversal processes, both the perpendicular and the parallel alignments between the pinned interface spins and the rotating Fe spins, with the corresponding frustrations, at variance with 180°-DW processes.

Such enlarged sensitivity for 90°-DW processes to the AF spin configuration could also explain the larger prominence of the "peak" of E_{DW} at $T=T_b$ for the 90°-DW case compared to the 180°-DW case. Such a peak is typically ascribed to the reduction in the AF anisotropy close to T_b that favors an increased drag of the AF spins by the FM via the mutual exchange coupling. In our case, as stated above, it is more physically meaningful to connect the sample coercivity with the DW activation and propagation energies rather than with the system MAE. Accordingly, the drag of AF spins by the FM can be thought of in terms of AF domain walls being dragged by the FM DWs during the magnetization reversal

process. In correspondence of the drop in AF anisotropy near T_b, such AF DWs (necessarily perpendicular to the interface due to the limited thickness of the AF layer) apparently involve a larger number of AF spins. This increase in the amount of dragged spins is then correspondingly reflected in the observed increase in activation energy.

IV. CONCLUSION

In conclusion, we addressed the EB properties of self-organized nanopatterned Cr/Fe junctions characterized by an atomic-scale-tailored FM-AF interface. The well-characterized system morphology, magnetic anisotropy, and magnetization reversal process made it possible to clearly correlate the interface atomic configuration with the exchange bias properties. In particular we were able to derive from our data the specific activation energy for different types of domain walls in our system and unveil a characteristic difference between the activation energy of 90° DW and 180° DW that we ascribe to the occurrence of geometrical spin frustrations in the sample.

Concerning the origin of the exchange bias in our system, our data suggest the apparently null role of $[001]_{Fe}$-aligned steps in providing uncompensated pinned spins at the interface, irrespective of the relative angle between $\mathbf{H}_{FC}$ and the ripple orientation. We therefore propose that morphological defects of the ripple structure are the most favorable locations at which the pinned uncompensated spins responsible for exchange bias are found. In order to further delve into the basic mechanisms of exchange bias in our ion-sculpted samples, particularly concerning the microscopic spin arrangement at the interface, it would be surely interesting to vary in a controlled manner the number of exposed Cr/Fe interface layers. Within this framework, great care will have to be taken in the data interpretation to clearly disentangle microscopic effects due to interface spin arrangements from the necessarily correlated influence of the long-range evolution of the ripple morphology. Finally, we suggest that the atomic-scale engineering of the interface for other FM-AF combinations might also prove useful for highlighting specific interfacial defects or morphological configurations responsible for EB with a great scientific and applicative potential.

ACKNOWLEDGMENTS

Financial support from the Università di Genova (PRA 2007) and the Fondazione Carige is acknowledged. F.B. acknowledges the CNR-CNISM convention for financial support.

*bisio@fisica.unige.it

[1] W. H. Meiklejohn and C. P. Bean, Phys. Rev. **102**, 1413 (1956).
[2] J. Nogués and I. K. Schuller, J. Magn. Magn. Mater. **192**, 203 (1999).
[3] J. Unguris, R. J. Celotta, and D. T. Pierce, Phys. Rev. Lett. **67**, 140 (1991).
[4] J. Nogués, J. Sort, V. Langlais, V. Skumryev, S. Suriñach, J. S. Muñoz, and M. D. Baró, Phys. Rep. **422**, 65 (2005).
[5] A. P. Malozemoff, Phys. Rev. B **35**, 3679 (1987).
[6] N. C. Koon, Phys. Rev. Lett. **78**, 4865 (1997).
[7] I. P. Krug, F. U. Hillebrecht, M. W. Haverkort, A. Tanaka, L. H. Tjeng, H. Gomonay, A. Fraile-Rodríguez, F. Nolting, S. Cramm, and C. M. Schneider, Phys. Rev. B **78**, 064427 (2008).
[8] J. Nogués, D. Lederman, T. J. Moran, I. K. Schuller, and K. V. Rao, Appl. Phys. Lett. **68**, 3186 (1996).
[9] S. H. Chung, A. Hoffmann, and M. Grimsditch, Phys. Rev. B **71**, 214430 (2005).
[10] J. Camarero, J. Sort, A. Hoffmann, J. M. García-Martín, B. Dieny, R. Miranda, and J. Nogués, Phys. Rev. Lett. **95**, 057204 (2005).
[11] M. O. Liedke, B. Liedke, A. Keller, B. Hillebrands, A. Mücklich, S. Facsko, and J. Fassbender, Phys. Rev. B **75**, 220407(R) (2007).
[12] S. E. Inderhees, J. A. Borchers, K. S. Green, M. S. Kim, K. Sun, G. L. Strycker, and M. C. Aronson, Phys. Rev. Lett. **101**, 117202 (2008).
[13] U. Valbusa, C. Boragno, and F. Buatier de Mongeot, J. Phys.: Condens. Matter **14**, 8153 (2002).
[14] F. Bisio, S. Terreni, M. Canepa, and L. Mattera, Phys. Rev. B **72**, 174413 (2005).
[15] D. E. Bürgler, C. M. Schmidt, D. M. Schaller, F. Meisinger, R. Hofer, and H.-J. Güntherodt, Phys. Rev. B **56**, 4149 (1997).
[16] F. Bisio, A. Toma, R. Moroni, R. Pasero, F. Buatier de Mongeot, C. Boragno, M. Canepa, U. Valbusa, and L. Mattera, Phys. Rev. B **75**, 054407 (2007).
[17] M. Canepa, S. Terreni, P. Cantini, A. Campora, and L. Mattera, Phys. Rev. B **56**, 4233 (1997).
[18] F. Bisio, R. Moroni, A. Chincarini, M. Canepa, and L. Mattera, J. Appl. Phys. **104**, 033905 (2008).
[19] R. Pfandzelter, T. Igel, and H. Winter, Surf. Sci. **375**, 13 (1997).
[20] R. P. Cowburn, S. J. Gray, J. Ferré, J. A. C. Bland, and J. Miltat, J. Appl. Phys. **78**, 7210 (1995).
[21] W. Weber, R. Allenspach, and A. Bischof, Appl. Phys. Lett. **70**, 520 (1997).
[22] F. Bisio, R. Moroni, F. Buatier de Mongeot, M. Canepa, and L. Mattera, Phys. Rev. Lett. **96**, 057204 (2006).
[23] F. Bisio, R. Moroni, F. Buatier de Mongeot, M. Canepa, and L. Mattera, Appl. Phys. Lett. **89**, 052507 (2006).
[24] J. Pommier, P. Meyer, G. Pénissard, J. Ferré, P. Bruno, and D. Renard, Phys. Rev. Lett. **65**, 2054 (1990).
[25] R. M. Osgood III, S. D. Bader, B. M. Clemens, R. L. White, and H. Matsuyama, J. Magn. Magn. Mater. **182**, 297 (1998).
[26] V. I. Nikitenko, V. S. Gornakov, L. M. Dedukh, Y. P. Kabanov, A. F. Khapikov, A. J. Shapiro, R. D. Shull, A. Chaiken, and R. P. Michel, Phys. Rev. B **57**, R8111 (1998).
[27] W.-T. Lee, S. G. E. te Velthuis, G. P. Felcher, F. Klose, T. Gredig, and E. D. Dahlberg, Phys. Rev. B **65**, 224417 (2002).
[28] M. R. Fitzsimmons, P. Yashar, C. Leighton, I. K. Schuller, J. Nogués, C. F. Majkrzak, and J. A. Dura, Phys. Rev. Lett. **84**, 3986 (2000).

[29] H. D. Chopra, D. X. Yang, P. J. Chen, H. J. Brown, L. J. Swartzendruber, and W. F. Egelhoff, Jr., Phys. Rev. B **61**, 15312 (2000).
[30] J. S. Parker, L. Wang, K. A. Steiner, P. A. Crowell, and C. Leighton, Phys. Rev. Lett. **97**, 227206 (2006).
[31] R. W. Sharp and P. C. Archibald, J. Appl. Phys. **37**, 1462 (1966).
[32] K.-Y. Kim, Y.-S. Hwang, J.-G. Park, N. Torikai, M. Takeda, S. W. Han, and S.-C. Shin, Phys. Status Solidi B **244**, 4499 (2007).
[33] H. Hopster, Phys. Rev. Lett. **83**, 1227 (1999).
[34] E. J. Escorcia-Aparicio, H. J. Choi, W. L. Ling, R. K. Kawakami, and Z. Q. Qiu, Phys. Rev. Lett. **81**, 2144 (1998).
[35] R. Robles, E. Martínez, D. Stoeffler, and A. Vega, Phys. Rev. B **68**, 094413 (2003).
[36] H. Ohldag, A. Scholl, F. Nolting, E. Arenholz, S. Maat, A. T. Young, M. Carey, and J. Stöhr, Phys. Rev. Lett. **91**, 017203 (2003).
[37] F. Radu, A. Nefedov, J. Grabis, G. Nowak, A. Bergmann, and H. Zabel, J. Magn. Magn. Mater. **300**, 206 (2006).
[38] M. Grimsditch, A. Hoffmann, P. Vavassori, H. Shi, and D. Lederman, Phys. Rev. Lett. **90**, 257201 (2003).
[39] V. I. Nikitenko, V. S. Gornakov, A. J. Shapiro, R. D. Shull, K. Liu, S. M. Zhou, and C. L. Chien, Phys. Rev. Lett. **84**, 765 (2000).